Carbohydrate Polymers 262 (2021) 117949

Contents lists available at ScienceDirect

Carbohydrate Polymers

journal homepage: www.elsevier.com/locate/carbpol

Stimuli-responsive flexible membrane via co-assembling sodium alginate into assembly membranes of rod-like cellulose nanocrystals with an achiral array

Xuhong Wang [a,1], Na Feng [a,1], Zhenxu Shi [a], Na Zhou [b], Jun Lu [c], Jin Huang [a,b,d,*], Lin Gan [a,d,*]

[a] School of Chemistry and Chemical Engineering, and Chongqing Key Laboratory of Soft-Matter Material Chemistry and Function Manufacturing, Southwest University, Chongqing 400715, PR China
[b] School of Chemistry and Chemical Engineering, and Engineering Research Center of Materials-Oriented Chemical Engineering of Xinjiang Bintuan, Shihezi University, Shihezi 832003, PR China
[c] College of Food Science & Chemical Engineering, Hubei University of Arts and Science, Xiangyang 441003, PR China
[d] Joint International Research Laboratory of Biomass-Based Macromolecular Chemistry and Materials, Chongqing 400715, PR China

ARTICLE INFO

Keywords:
Cellulose nanocrystal
Assembly-induced emission
Achiral assembly
Flexible sensor

ABSTRACT

Uniaxially assembling cellulose nanocrystals (CNCs) can induce strong solid-state emission based on optical inelastic scattering, whereas the CNC assembly membranes are not flexible enough for further applications. Thus, we introduced CNC into flexible sodium alginate (SA) and further controlled the assembly structure of CNC to increase the membrane toughness and maintain the emission properties. The results indicated that the stretchability increased from 0.027 % to 37 % when 33–37% when 33 % SA was introduced. The assembly achirality was controlled by tuning CNC concentration in suspension, and the co-assembly could further control the wavelength of the assembly-induced emission from 420 nm to 440 nm. Furthermore, the improved stretchability made assembly membrane an optical sensor, whose excitation wavelength blue-shifted about 30 nm under a 30 % strain. The emission of the co-assembly membrane could also respond to humidity, and this cellulose-based material should have great potential in biosensor and wearable devices.

1. Introduction

Cellulose nanocrystals (CNCs) can assemble in a chiral nematic structure (Andrea, Wadood, & Mark, 2017; Bharath et al., 2018; Hausmann et al., 2018) or an achiral aligning structure (Gan et al., 2019) to present structural colors (Bardet, Belgacem, & Bras, 2015; Hiratani, Hamad, & MacLachlan, 2017), which have great application potential in information encryption (Majoinen et al., 2016; Yang, Wang, Huang, Cui, & Zhang, 2020), anti-counterfeiting (Peixi, Wadood, & Mark, 2016; Philippe, Tanja, & Gilles, 2012), and sensors (Salas, Nypel, Rodriguez-Abreu, Carrillo, & Rojas, 2014; Zhao et al., 2017). However, their application is limited, especially in the field of flexible sensors, due to the brittleness and low ductility of the optical materials prepared from cellulose nanocrystals (Fortunati et al., 2012; Lasemi, Xue, & Gu, 2010; Leng et al., 2018).

The disadvantages of CNC-based photonic materials can be overcome by co-assembling it with a flexible substrate (Guidetti, Atifi, Vignolini, & Hamad, 2016; Shopsowitz, Hamad, & MacLachlan, 2012; Yao, Meng, Bulone, & Zhou, 2017). For example, co-assembly of CNCs and flexible substrate aqueous glutaraldehyde (GA) resulted in membranes that were very flexible, and which could bend and roll without cracking (Hanif, Choi, Tariq, La, & Park, 2020). Also, composite membranes containing silicone-modified acrylic latices and CNCs prepared by evaporation induced self-assembly, can have high flexibility and adjustable structure colors (Leng et al., 2018).

Unfortunately, these co-assemble methods mostly result in chiral structures instead of achiral ones, leading to iridescence and no emission ability, in which the iridescence must decrease the sensitivity of those sensors (Bardet et al., 2015; Lizundia, Nguyen, & Vilas, 2017; Meng et al., 2020). This is because the optical signals of iridescence vary uncontrollably with a slight change in the observing angle or position. For example, with co-assembly CNCs and polyethylene glycol (PEG), a chiral

* Corresponding authors at: School of Chemistry and Chemical Engineering, and Chongqing Key Laboratory of Soft-Matter Material Chemistry and Function Manufacturing, Southwest University, Chongqing 400715, PR China.
E-mail addresses: huangjin2015@swu.edu.cn (J. Huang), swucgl@swu.edu.cn (L. Gan).
[1] Xuhong Wang and Na Feng equally.

https://doi.org/10.1016/j.carbpol.2021.117949
Received 13 October 2020; Received in revised form 10 March 2021; Accepted 12 March 2021
Available online 17 March 2021
0144-8617/

nanocomposite photonic membrane can be prepared (Carosio, Cuttica, Medina, & Berglund, 2016). By controlling the co-assembly structure, a structural color similar to monochromatic can be formed, but the imperfection of monochromatic is still insufficient for application in sensing. Besides, by combining CNC and PVA, iridescence materials with chiral structure have been prepared, which could have applications in the field of flexible sensing by reflecting color (Song, Liu, Prempeh, & Song, 2017). However, the unknown dominance of reflected color still made them inefficient in sensors.

Hence, we introduced SA into the CNC system and prepared CNC/SA flexible membrane with achiral structure by evaporation-induced vertical assembly. The achirality of the CNC/SA co-assembly was controlled via adjusting the CNC/SA ratio. Then, we studied the effect of assembly structure on the mechanical properties of CNC/SA membrane. Meanwhile, the stimuli-responsiveness was investigated by measuring the changes in CNC/SA membranes in emission properties under bending and stretching. We also studied the influence of humidity on the emission of CNC/SA membranes. It is hypothesized that since the cellulose/SA-based carbohydrate membranes were found to own high toughness and emission properties responding to mechanical stimuli and humidity, they should have great potential in optical sensors and information security.

2. Experimental sections

2.1. Materials

Cotton linter was purchased from Hubei Chemical Fiber Group Co., Ltd. (China). Sodium alginate (SA, CP, $Mn = 1.26*10^6$, Viscosity 200 ± 20 mpa.s) was purchased from Shanghai Macklin Biochemical Co., Ltd. (China), the mannuronate : guluronate ratio of SA was 1:1. Sodium hydroxide (NaOH) and sulfuric acid (H_2SO_4, 98 %) were purchased from Chongqing Chuandong Chemical (Group) Co., Ltd. (China).

2.1.1. Extraction of cellulose nanocrystals (CNCs)

Cotton linter was used as raw materials, and CNCs with sulfonic acid groups on their surface were obtained by H_2SO_4 hydrolysis (Li, Wang, Long, Gan, & Huang, 2020). First, 50 g cotton linters were immersed in 2.0 L of a 2 wt% NaOH solution and stirred at room temperature (25℃) for 12 h to remove lignin and hemicellulose. Then the product was washed to pH neutrality and dried at 45℃. Subsequently, 12.5 g of the product was weighed into a three-necked flask, 250 mL of 65 wt% H_2SO_4 was added and mechanically stirred at 45℃ for 60 min to hydrolyze the amorphous region of cellulose fiber. After the reaction was completed, the mixture was cooled with a large amount of ice water to terminate the hydrolysis of CNC. The white dispersion so obtained was centrifuged at 4000 rpm for 5 min to remove H_2SO_4, and washed by three times with distilled water. Finally, the suspension was collected into a dialysis bag (The maximum molecular weight *M*n of the molecules allowed to penetrate is 15000.) and dialyzed to neutrality (3–5 days) to obtain CNC suspension.

2.1.2. Preparation of CNC/SA flexible membrane

In this study, CNCs obtained by H_2SO_4 hydrolysis were introduced into SA, and uniaxial assembled membrane was prepared as follows. Firstly, the concentration of CNC suspension was adjusted to 0.1 wt%, 0.2 wt%, 0.5 wt%, 1.0 wt%, 2.0 wt%, 3.0 wt%, 4.0 wt%, respectively; and the suspension was added into an aqueous solution of 2 wt% SA. Then, 10 mL CNC/SA suspension was placed in a 20 mL clean glass bottle, and a plasma-cleaned glass sheet was inserted vertically into the bottle keeping it perpendicular to the bottom of the bottle. The glass bottle was placed in a constant temperature and humidity box with less vibration, and the temperature was at 30 °C and the humidity at 30 %. Finally, as the solvent evaporated, a CNC/SA uniaxial assembled membrane was obtained on the glass slide. The obtained CNC/SA vertical self-assembled membrane was immersed in 2% $CaCl_2$ solution to make it fully cross-linked to obtain a CNC/SA uniaxial assembled flexible membrane. Based on the concentration of CNC in the CNC/SA uniaxial assembled flexible membrane, the samples were coded as CNC/SA-x, where the "x" is the mass percentage in the CNC suspension.

2.2. Characterization of the CNC/SA uniaxial assembled membrane

2.2.1. Atomic force microscope test (AFM)

The CNC/SA uniaxial assembled membrane sample was fixed on the sample stage, and the lightweight mode was used as the test mode. The TEPSA probe was selected for AFM (Bruker, Germany) test.

2.2.2. Fluorescence spectrometer test (FL)

The samples of different surface-modified CNC assembly membranes were fixed on the sample holder, and the test was performed with a 5JI-004 (Hitachi High-technologies corporation) fluorescence spectrometer in solid mode.

2.2.3. Tensile test

The tensile properties of the assembled membrane materials were tested using a computer-controlled electronic universal testing machine (CMT5503, Shenzhen Sansi Aspect Technology Co., Ltd.) to characterize the tensile properties of the CNC/SA uniaxial assembled stretchable membrane.

3. Results and discussions

3.1. Morphology and the angle orientation of different CNC/SA flexible membranes

Atomic force microscopy (AFM) was used to analyze the achiral degree of cellulose nanocrystals (CNCs) in sodium alginate (SA), and the typical AFM phase image is shown in Fig. 1a. The included angle (θ) between CNC long-axis and vertical direction in the CNC uniaxial assembled membrane was measured and the statistical data is shown in Fig. 1b–h. Then the achiral degree was calculated as the orientation degree with Eq. (1)

$$F = \frac{1}{2}\left(3\left\langle\cos^2\theta\right\rangle - 1\right) \quad (1)$$

where *F* is the orientation degree. The result showed that F varied in a narrow region between 39 and 58 after CNC co-assembled with SA, which meant that the uniaxial assembly structure still existed in the CNC/SA uniaxial assembled flexible membrane. The result also showed that the *F* reached the maximum value of 0.9787 with CNC/SA-1.0.

3.2. Effect of co-assembly with SA on the mechanical and optical properties of CNC array

Tensile tests were used to measure the flexibility of CNC/SA membranes, as shown in Fig. 2a. The result showed that the yield strength of the membranes decreased from 8.5 MPa to 1 MPa, as the SA content increased from 0 to 66 %. Meanwhile, the elongation at break and the toughness of the membrane reached the maximal value 37 % and 372 J/cm^2, respectively, when the SA content was 66 %. These results indicated that co-assembling with SA could improve the flexibility and toughness of CNC-array membranes.

As mentioned above, the uniaxial assembly structure of CNC could be extended into CNC/SA flexible membrane, which meant the combination of CNC and SA should still maintain the photoluminescence (PL) properties. The PL spectra of CNC/SA flexible membranes at different ratios are shown in Fig. 3. The results of PL spectroscopy analysis showed that the excitation wavelengths of the CNC/SA flexible membranes obtained at different ratios were all at 380 nm. According to the previous research results (Gan et al., 2019), this PL phenomenon was

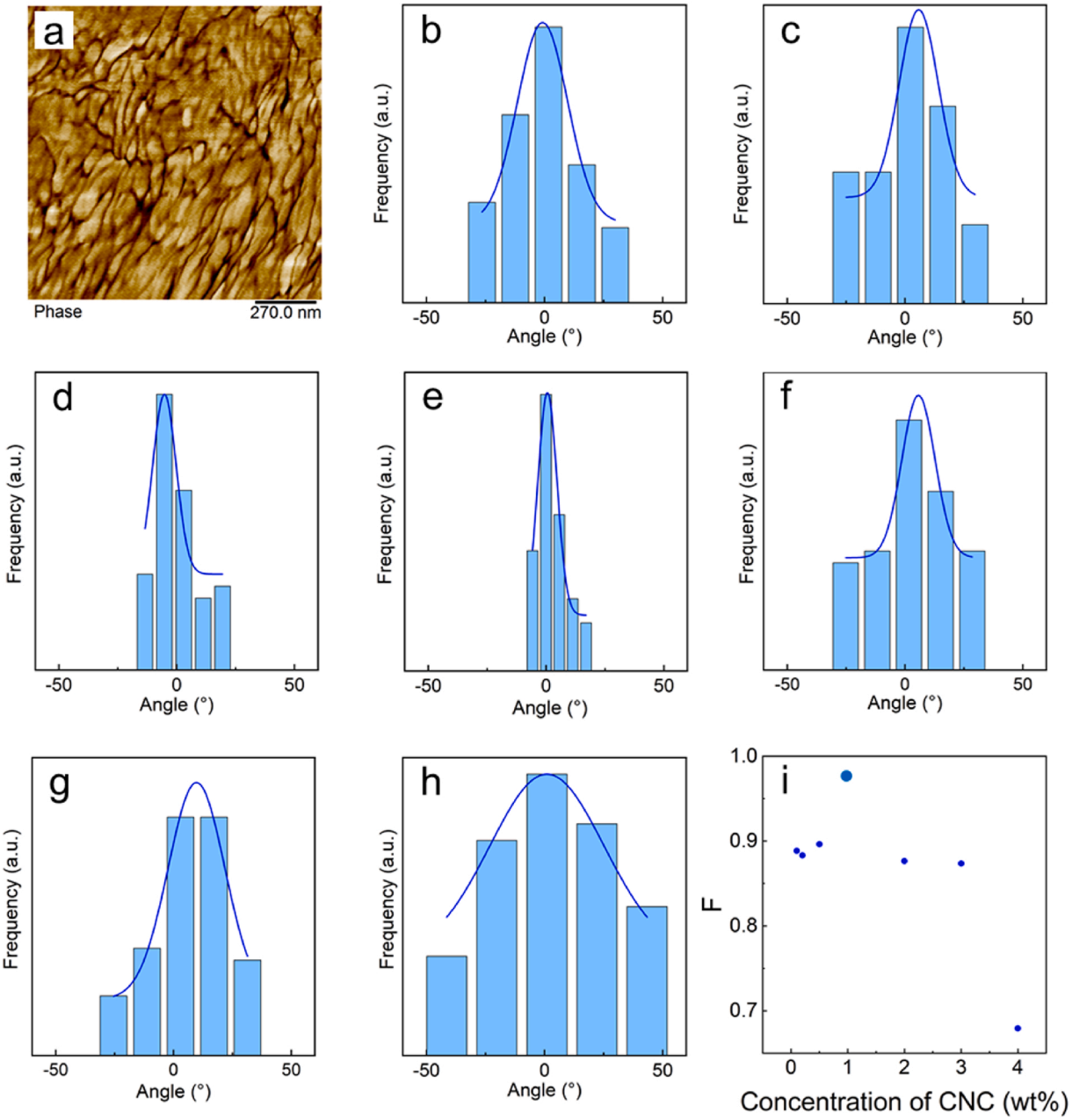

Fig. 1. (a) Typical AFM image of the cellulose nanocrystals/sodium alginate (CNC/SA) co-assembly membrane (here the CNC concentration is 1.0 wt%). The distribution of the included angle between CNC long-axis and vertical direction in the CNC uniaxial assembled membrane that were prepared with CNC concentration of (b) 0.1 wt %, (c) 0.2 wt %, (d) 0.5 wt %, (e) 1.0 wt %, (f) 2.0 wt %, (g) 3.0 wt % and (h) 4.0 wt %. (i) The relationship between the orientation degree of CNC and CNC concentration.

caused by the uniaxial assembly of CNC, and the change in PL peak might be attributed to in the change in effective refractive index (*n*) from the introduced SA.

3.3. Mechanical responsiveness of CNC/SA flexible membranes

The PL-responsiveness on stretching and bending is shown in Figs. 4 and 5, respectively. The result indicated that the excitation wavelength of CNC/SA-1.0 decreased from 380 nm to 360 nm as the tensile strain increased from 0 to 30 %. The emission peak at 420 nm gradually disappeared until the tensile strain was 30 % after which it disappeared completely. Furthermore, the emission intensity of the co-assembly membrane increased obviously on the stress (Fig. 4c and d). Meanwhile, the excitation wavelength of CNC/SA-1.0 increased from 380 nm to 364 nm as the bending strain increased from 180° to 109°, and the emission peak at 450 nm gradually disappeared until the bending strain was 109° after which it disappeared completely. The PL responsiveness on mechanical strain should be ascribed to the change in achiral degree that was induced by stress, because the increase in achiral degree could induce a wideness in the photon band gap of the photonic crystal based on rod-like CNC particles (Dai, Wang, Chen, Li, & Zhou, 2012; Krishnamoorthy, Jacob, Narimanov, Kretzschmar, & Menon, 2012; Lagerwall et al., 2014).

The Bragg-diffraction (λ_{Bragg}) wavelength of CNC assembled uniaxially could be expressed by Eq. (2)

$$\mathrm{m}\ \lambda_{Bragg} = 2D\sqrt{n_{eff}^2 - sin^2\theta} \quad (2)$$

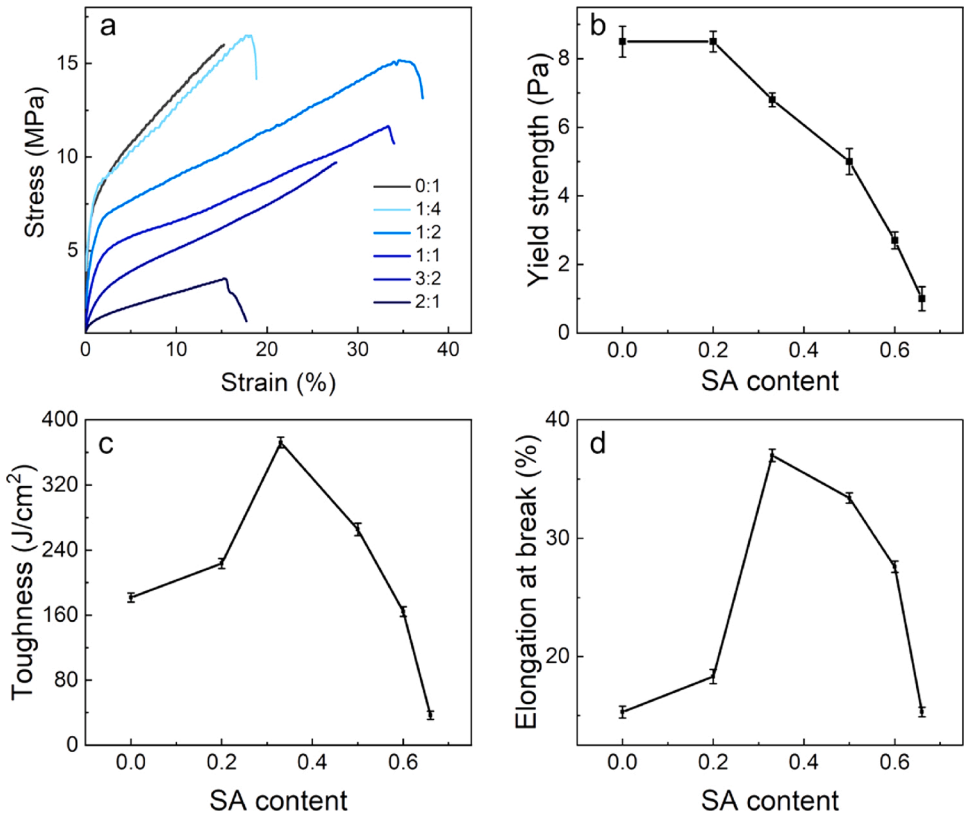

Fig. 2. (a) Stress-strain curves of cellulose nanocrystals/sodium alginate (CNC/SA) co-assembly membranes with different mass ratios of CNC:SA. The (b) yield strength, (c) toughness, and (d) elongation at break of CNC/SA co-assembly membranes with different SA contents.

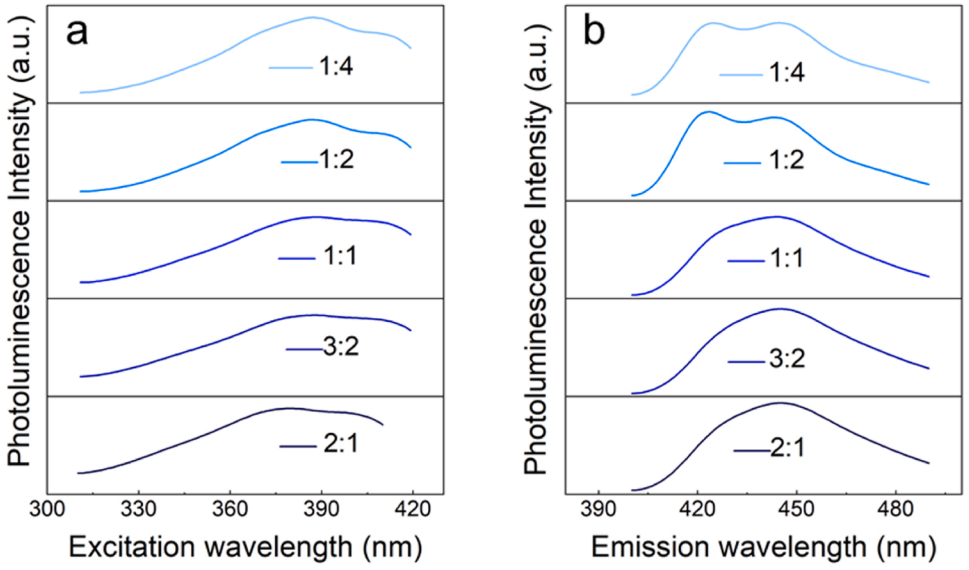

Fig. 3. (a) Excitation spectra and (b) emission spectra of cellulose nanocrystals/sodium alginate (CNC/SA) co-assembly membranes with different mass ratios of CNC:SA.

where λ_{Bragg} is the wavelength of Bragg diffraction, m is the diffraction order, n_{eff} is the effective refractive index, and θ is the incident angle, D is the vertical periodicity (Gan et al., 2019). The n_{eff} was calculated with Eq. (3) (Yamasaki & Tsutsui, 1998; Zhao, Xie, Gu, Zhu, & Gu, 2012)

$$n_{eff}^2 = V_{CNC}\, n_{CNC}^2 + V_{SA}\, n_{SA}^2 \quad (3)$$

where n_{CNC} and n_{SA} are the refractive indices of CNC (1.534, Cranston & Gray, 2008) and SA (1.342, Prakash, Ramakrishna, & Rai, 2003), respectively. The V_{CNC} and V_{SA} are the volume fraction of CNC and SA, which could be calculated by Eq. (4)

$$\rho_M\, V = \rho_{CNC}\, V_{CNC} + \rho_{SA}\, V_{SA} \quad (4)$$

where ρ_M, ρ_{CNC} and ρ_{SA} are density of co-assembly membrane, CNC (1.56, Paralikara, Simonsen, & Lombardi, 2008) and SA (1.0), respectively. The density of ρ_M was 1.444, so the V_{CNC} and V_{SA} were 79 % and 21 %, respectively.

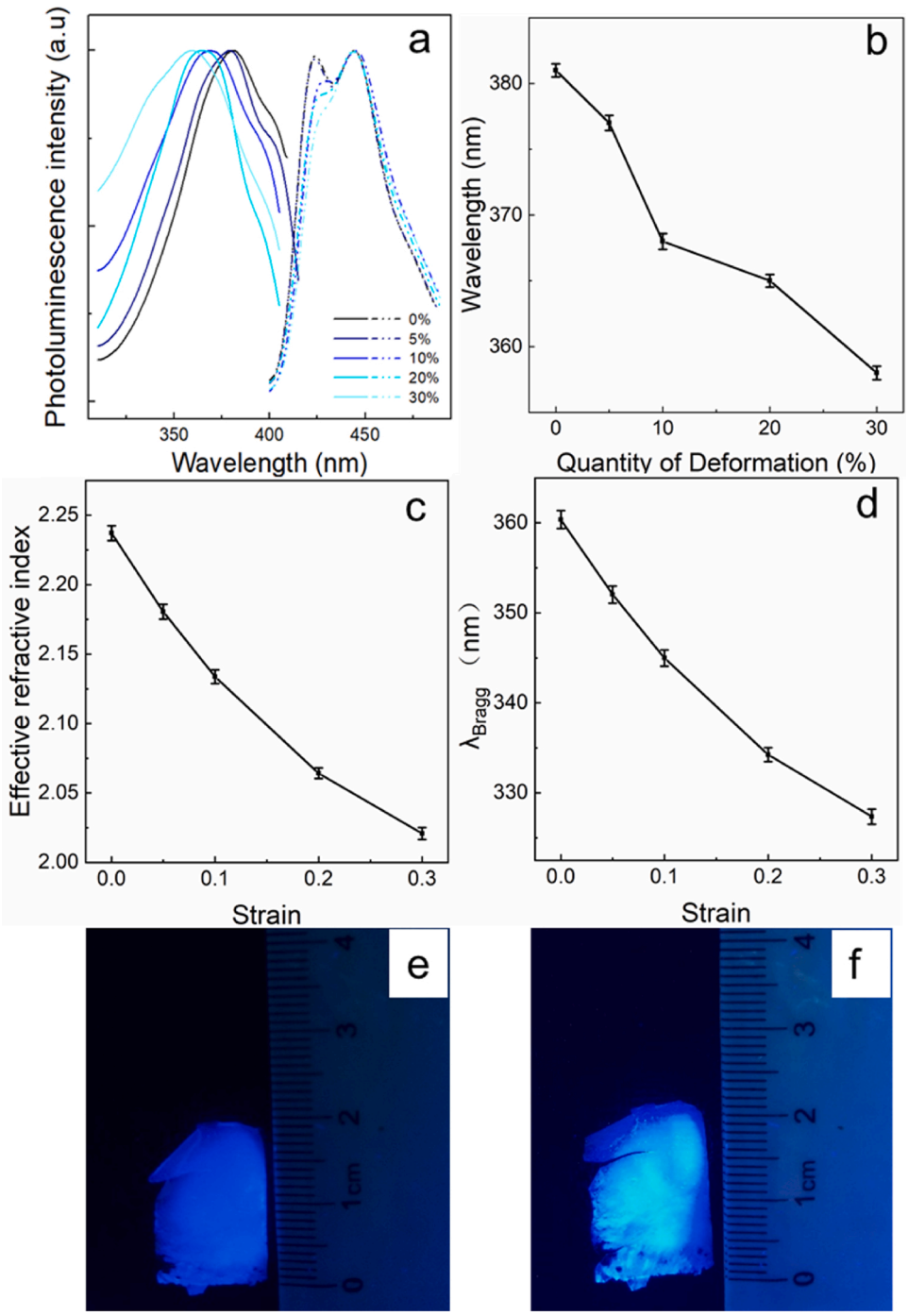

Fig. 4. (a) Excitation spectra (full lines) and emission spectra (break lines) of cellulose nanocrystals/sodium alginate (CNC/SA-1.0) membrane under different tensile strains. (b) Relationship between the excitation wavelength and tensile strain of CNC/SA-1.0 membrane. Relationship between the theoretical (c) effective refractive index, (d) effective Bragg-diffraction wavelength and tensile strain of CNC/SA-1.0 membrane. The photographs of CNC/SA-1.0 membrane under 365 nm UV light with tensile strains of (e) 0% and (f) 5%.

Thus, the n_{eff} of CNC/SA co-assembly membrane after stretching was calculated with Eq. (5)

$$n_{eff}^2 = V_{CNC}\, n_{CNC}^2 + V_{SA}\, n_{SA}^2 + V_{air}\, n_{air}^2 \quad (5)$$

where V_{air} is volume fraction of air in the membrane, which was equal to the strain of CNC/SA co-assembly membrane; and n_{air} is the refractive indices of air (1.0). Fig. 4c indicated the relationship between the n_{eff} and different strains.

In this study, the value of m was 1; the detecting direction was perpendicular to the CNC assembled uniaxially membrane, which meant the θ was 90°, so the value of $\sin^2\theta$ was 1. D was approximately regarded as the length of CNC (162 nm). Thus, the relationship between λ_{Bragg} and strain was shown in Fig. 4d. There is an error between the theoretical value and the actual value. However, the change in the n_{eff} of the material causes this stimuli-responsible membrane.

3.4. Humidity response of CNC/SA flexible membrane

The PL-response on humidity is shown in Fig. 6. The result indicated that the emission peaks at 447 nm of CNC/SA-1.0 was improved under humidity condition. In a stretched state of 30 % strain, the improvement was *ca.* 5 %, while in a bending state of 180°, the improvement was *ca.* 3 %. Furthermore, the intensity ratio between peaks at 420 nm and 447 nm increased when the film was wet. The increment was 15 % and 13 % at the stretched state and the bending state, respectively. The PL-response on humidity might be attributed to the change the effective refractive index (n) of CNC/SA stretchable membrane, in which SA had

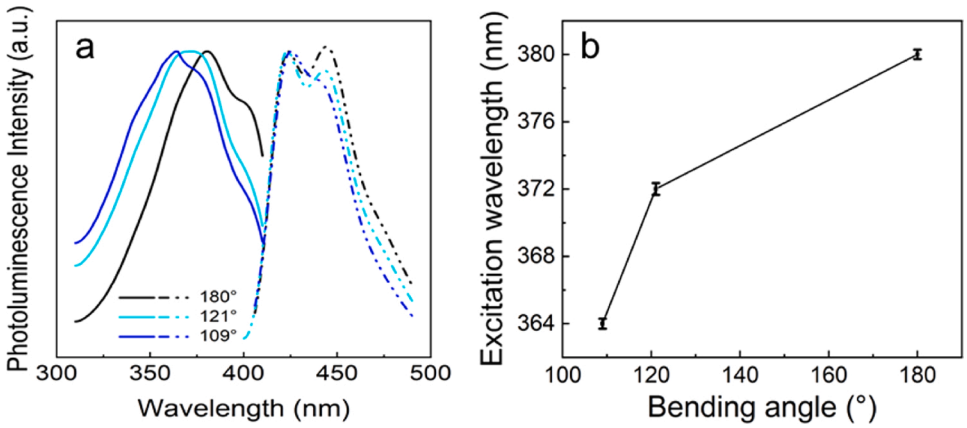

Fig. 5. (a) Excitation spectra (full lines) and emission spectra (break lines) of cellulose nanocrystals/sodium alginate (CNC/SA-1.0) membrane under different bending angles. (b) Relationship between the excitation wavelength and angle of bend of CNC/SA-1.0 membrane.

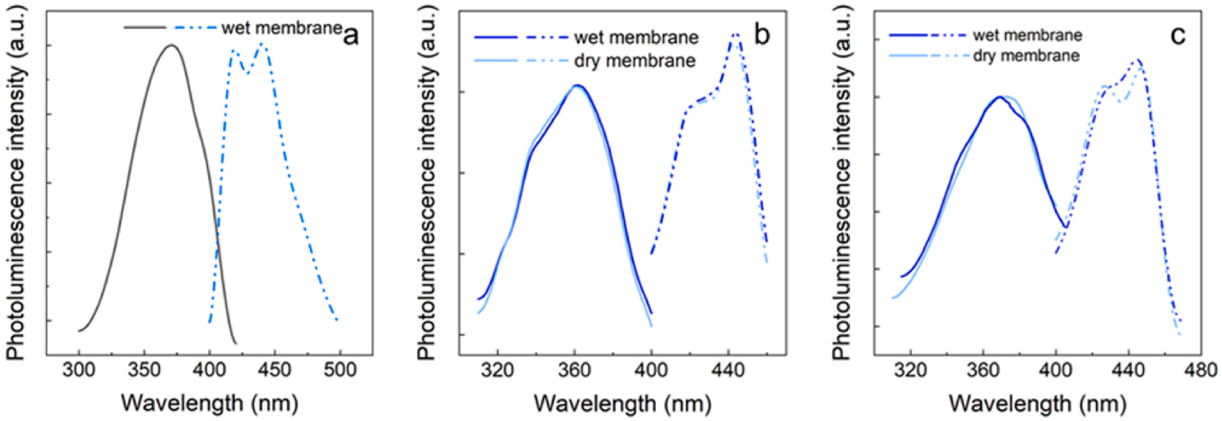

Fig. 6. (a) Excitation spectrum (full line) and emission spectrum (break line) of cellulose nanocrystals/sodium alginate (CNC/SA-1.0) membrane under wet state. (b) Excitation spectrum (full line) and emission spectrum (break line) of CNC/SA-1.0 membrane with a tensile strain of 30 % under wet (blue) and dry state (light blue). (c) Excitation spectrum (full line) and emission spectrum (break line) of CNC/SA-1.0 membrane with a bending angle of 121° under wet (blue) and dry state (light blue).

water absorption and led to a decrease in *n* of SA part and an increase in the photon band gap (Gan et al., 2019).

4. Conclusions

We introduced flexible sodium alginate (SA) into cellulose so obtained nanocrystal (CNC) membrane and controlled the assembly structure and assembly-induced emission of CNC by adjusting their co-assembly process. The achiral degree of assembling CNC array reached the maximum when the mass ratio between CNC and SA was 1:1, with an orientation degree (*F*) of 0.9787. The CNC/SA membrane so obtained showed improved elongation at break and toughness of 37 % and 372 J/cm^2, respectively. Also, the yield strength of the CNC/SA membrane decreased from 8.5 MPa to 1 MPa when 66 wt% SA was introduced. The membrane was flexible, and demonstrated blue shift on stretching and bending. The blue-shift degree was linear with the stretching strain, and maximal shift wavelength was ca. 30 nm. Meanwhile, the emission spectrum of CNC/SA membrane varied by ca. 5 % when the membrane was wet, suggesting that the optical membrane could also respond to the humidity. Such a flexible optical sensor based on achiral CNC assembly in flexible polymers can promote its application in biosensors and optical anti-counterfeiting in paper-based materials.

CRediT authorship contribution statement

Xuhong Wang: Conceptualization, Methodology, Investigation, Writing - original draft. **Na Feng:** Conceptualization, Methodology, Investigation, Writing - original draft. **Zhenxu Shi:** Methodology, Data curation, Investigation. **Na Zhou:** Data curation, Investigation. **Jun Lu:** Data curation, Supervision. **Jin Huang:** Conceptualization, Supervision, Project administration, Funding acquisition. **Lin Gan:** Conceptualization, Methodology, Writing - review & editing, Visualization.

Acknowledgements

This research is financially supported by the National Natural Science Foundation of China (51973175), the Fundamental Research Funds for the Central Universities (XDJK2019TY002), the Project for Chongqing University Innovation Research Group of Chongqing Education Committee (CXQT19008), the Chongqing Talent Plan for Innovation and Entrepreneurship Demonstration Team (CQYC201903243), and the S&T Project of Science and Technology Bureau of Bishan District in Chongqing (Bskj20200011).

Appendix A. Supplementary data

Supplementary material related to this article can be found, in the online version, at doi:https://doi.org/10.1016/j.carbpol.2021.117949.

References

Andrea, S. T., Wadood, Y. H., & Mark, J. M. (2017). Photopatterning freestanding chiral nematic mesoporous organosilica membranes. *Advanced Functional Materials, 27*(45), Article 1703346.

Bardet, R., Belgacem, N., & Bras, J. (2015). Flexibility and color monitoring of cellulose nanocrystal iridescent solid membranes using anionic or neutral polymers. *ACS Applied Materials & Interfaces, 7*(7), 4010–4018.

Bharath, N., Ajay, K., Xin, Q., Caglar, D. E., Amanda, F., Johan F, E., et al. (2018). Binary cellulose nanocrystal blends for bioinspired damage tolerant photonic membranes. *Advanced Functional Materials, 28*, Article 1800032.

Carosio, F., Cuttica, F., Medina, L., & Berglund, L. A. (2016). Clay nanopaper as multifunctional brick and mortar fire protection coating-wood case study. *Materials & Design, 93*, 357–363.

Cranston, E. D., & Gray, D. G. (2008). Birefringence in spin-coated films containing cellulose nanocrystals. *Colloids and Surfaces A, Physicochemical and Engineering Aspects, 325*(1–2), 44–51.

Dai, W., Wang, H., Chen, S., Li, D., & Zhou, D. (2012). Effect of point defects on band-gap properties in diamond structure photonic crystals. *Journal of Applied Physics, 111*(2), 2486.

Fortunati, E., Armentano, I., Zhou, Q., Iannoni, A., Saino, E., Visai, L., et al. (2012). Multifunctional bionanocomposite films of poly (lactic acid), cellulose nanocrystals and silver nanoparticles. *Carbohydrate Polymers, 87*(2), 1596–1605.

Gan, L., Feng, N., Liu, S., Zheng, S., Li, Z., & Huang, J. (2019). Assembly-induced emission of cellulose nanocrystals for hiding information. *Particle & Particle Systems Characterization, 36*(3), Article 1800412.

Guidetti, G., Atifi, S., Vignolini, S., & Hamad, W. Y. (2016). Flexible photonic cellulose nanocrystal films. *Advanced Materials, 28*(45), 10042–10047.

Hanif, Z., Choi, D., Tariq, M. Z., La, M., & Park, S. J. (2020). Water-stable flexible nanocellulose chiral nematic films through acid vapor cross-linked glutaraldehyde for chiral nematic templating. *ACS Macro Letters, 9*(2), 146–151.

Hausmann, M. K., Rühs, P. A., Siqueira, G., Läuger, J., Libanori, R., Zimmermann, T., et al. (2018). Dynamics of cellulose nanocrystal alignment during 3D printing. *ACS Nano, 12*(7), 6926–6937.

Hiratani, T., Hamad, W. Y., & MacLachlan, M. J. (2017). Transparent depolarizing organic and inorganic films for optics and sensors. *Advanced Materials, 29*, Article 1606083.

Krishnamoorthy, H. N., Jacob, Z., Narimanov, E. E., Kretzschmar, I., & Menon, V. M. (2012). Topological transitions in metamaterials. *Science, 336*(6078), 205–209.

Yao, K., Meng, Q., Bulone, V., & Zhou, Q. (2017). Flexible and responsive chiral nematic cellulose nanocrystal/poly (ethylene glycol) composite membranes with uniform and tunable structural color. *Advanced Materials, 29*(28), Article 1701323.

Lagerwall, J. P., Schutz, C., Salajkova, M., Noh, J., Park, J. H., Scalia, G., et al. (2014). Cellulose nanocrystal-based materials: From liquid crystal self-assembly and glass formation to multifunctional thin films. *NPG Asia Materials, 6*(1), 1–12.

Lasemi, A., Xue, D., & Gu, P. (2010). Recent development in CNC machining of freeform surfaces: A state-of-the-art review. *Computer-Aided Design, 42*(7), 641–654.

Leng, J. X., Li, G. H., Ji, X. X., Yuan, Z. W., Fu, Y. J., Li, G. H., et al. (2018). Flexible latex photonic membranes with tunable structural colors templated by cellulose nanocrystals. *Journal of Materials Chemistry C, 6*(9), 2396–2406.

Li, D., Wang, Y., Long, F., Gan, L., & Huang, J. (2020). Solvation-controlled elastification and shape-recovery of cellulose nanocrystal-based aerogels. *ACS Applied Materials & Interfaces, 12*(1), 1549–1557.

Lizundia, E., Nguyen, T.-D., & Vilas, J. L. (2017). Chiroptical, morphological and conducting properties of chiral nematic mesoporous cellulose/polypyrrole composite films. *Journal of Materials Chemistry A, 5*(36), 19184–19194.

Majoinen, J., Hassinen, J., Haataja, J. S., Rekola, H. T., Kontturi, E., Kostiainen, M. A., et al. (2016). Chiral plasmonics using twisting along cellulose nanocrystals as a template for gold nanoparticles. *Advanced Materials, 28*(26), 5262–5267.

Meng, Y., Cao, Y., Ji, H., Chen, J., He, Z., Long, Z., et al. (2020). Fabrication of environmental humidity-responsive iridescent films with cellulose nanocrystal/polyols. *Carbohydrate Polymers, 240*, Article 116281.

Paralikara, S. A., Simonsen, & Lombardi. (2008). Poly (vinyl alcohol)/cellulose nanocrystal barrier membranes. *Journal of Membrane Science, 320*, 248–258.

Peixi, W., Wadood, Y. H., & Mark, J. M. (2016). Polymer and mesoporous silica microspheres with chiral nematic order from cellulose nanocrystals. *Angewandte Chemie International Edition, 55*(40), 12460–12464.

Philippe, T., Tanja, Z., & Gilles, S. (2012). Cellulose nanocrystals and microfibrillated cellulose as building blocks for the design of hierarchical functional materials. *Journal of Materials Chemistry, 22*(38), 20105.

Prakash, S., Ramakrishna, H., Rai, S., et al. (2003). Miscibility studies of sodium alginate/poly (vinyl alcohol) blend in water by viscosity, ultrasonic, and refractive index methods. *Journal of Applied Polymer Science, 90*, 33–39.

Salas, C., Nypel, T., Rodriguez-Abreu, C., Carrillo, C., & Rojas, O. J. (2014). Nanocellulose properties and applications in colloids and interfaces. *Current Opinion in Colloid & Interface Science, 19*(5), 383–396.

Shopsowitz, K. E., Hamad, W. Y., & MacLachlan, M. J. (2012). Flexible and iridescent chiral nematic mesoporous organosilica films. *Journal of the American Chemical Society, 134*(2), 867–870.

Song, W., Liu, D., Prempeh, N., & Song, R. (2017). Fiber alignment and liquid crystal orientation of cellulose nanocrystals in the electrospun nanofibrous mats. *Biomacromolecules, 18*(10), 3273–3279.

Yamasaki, T., & Tsutsui, T. (1998). Spontaneous emission from fluorescent molecules embedded in photonic crystals consisting of polystyrene microspheres. *Applied Physics Letters, 72*(16), 1957–1959.

Yang, Y., Wang, X., Huang, H., Cui, S., & Zhang, K. (2020). Modular nanocomposite films with tunable physical organization of cellulose nanocrystals for photonic encryption. *Advanced Optical Materials*, Article 2000547.

Zhao, Y., Xie, Z., Gu, H., Zhu, C., & Gu, Z. (2012). Bio-inspired variable structural color materials. *Chemical Society Reviews, 41*, 3297.

Zhao, Z., Wang, H., Shang, L., Yu, Y., Fu, F., Zhao, Y., et al. (2017). Bioinspired heterogeneous structural color stripes from capillaries. *Advanced Materials, 29*(46).